PHENOMENA OF DYNAMIC STALL ON SWEPT WINGS

Jens Henkner
Lehrstuhl für Fluidmechanik, TU München, Boltzmannstr. 15, 85747 Garching, Germany
now: Dornier Luftfahrt GmbH, Oberpfaffenhofen, P.O Box 1103, 82230 Wessling

Keywords: *boundary layer, three-dimensional, unsteady, separation*

Abstract

Surface pressure distributions on pitching swept wings show differences to equivalent two-dimensional cases. With the aid of a newly developed hot wire probe flow fields of a three-dimensional, unsteady boundary layer separation can be presented for the first time. The temporal evolution of the dynamic stall on a swept wing in sinusoidal motion is shown for a selected example. Comparative numerical results are principally in good agreement with the experiment. A refined generalized model for the onset of dynamic stall and the evolution of the vortex can be given from detailed analysis of the experimental and computational results. It becomes evident that the beginning of the stall is a process driven by boundary layer effects while the outer flow follows a quasi-steady progression until the onset of the dynamic stall vortex.

1 Nomenclature

c	chord length
f	frequency
k	reduced frequency $k = 2\pi f c/V_\infty$
Ma	Mach number
Re	Reynolds number
t	time
T	duration of a cycle
u	chordwise velocity component
v	spanwise velocity component
V	velocity $V = \sqrt{u^2+v^2+w^2}$
w	normal velocity component
n	off-wall distance
x	chordwise coordinate
y	spanwise coordinate
z	normal coordinate
α	incidence angle,
α_{ss}	incidence angle of static stall
β	yaw angle
β_{loc}	displacement angle (s. Fig. 2)
ω	angular velocity $\omega = 2\pi f$
∞	freestream quantities
$\uparrow$	upstroke motion
$\downarrow$	downstroke motion

2 Introduction

Over the last several decades unsteady stall phenomena have been topics of intensive research. It is well known that in two dimensional unsteady flow separation does occurs at greater incidence angles than in the steady case, attainable lift coefficients being significantly higher. This has been demonstrated by many surface pressure measurements e.g. [2, 3, 5]. Through flow visualization it becomes evident that this phenomena is caused by the evolution and shedding of the so called dynamic stall vortex. Flow field measurements [15, 14] have contributed to a more detailed insight into this process.

Essential contributions to the understanding of two-dimensional unsteady boundary layer separation were given by Ranke and Laschka [16, 15, 11] who are proposing a refined definition of unsteady boundary layer separation.

Under three dimensional conditions on swept wings, surface pressure measurements show similar effects to the two-dimensional setups. However the temporal evolution of the dynamic stall process is delayed [8]. This results into a lift cycle comparable to the two- dimensional case, yet at a higher reduced frequency. Due to the lack of flow field measurements no explanations for these observations could be given. Moreover no model for a three-dimensional, unsteady boundary layer separation and here in particular on swept wings has been established up till now.

The objective of the present study is to establish a refined theory for the evolution of the dynamic stall and the onset of the dynamic stall vortex for swept and unswept wings. The proposed model is based on measurements of the flowfield of a swept wing pitching in sinusoidal motion around its quarter chord line. The experimental flowfield data were obtained with the aid of a newly developed hot wire probe and the appropriate data processing. Comparative Navier-Stokes calculations of an infinite, swept wing with identical movement accompanied the experiments and contributed to a detailed spatial resolution while the experiments enabled a fine temporal resolution. Experiments and calculations were carried out at very low Mach numbers $Ma < 0.1$ with a Reynolds number of 250000 and reduced frequencies in the range from $k = 0.15$ to $k = 0.45$.

3 Experimental Setup

The experiments were conducted in a low speed windtunnel with a rectangular cross section of $1500x1200mm^2$ and an open test section which permits freestream velocities up to $60m/s$. The testbed consists of a rectangular wing, with a NACA0012 airfoil normal to leading edge, made out of carbon fibre reinforced plastic having a steel axle through the quarter chord. Supported by a steel frame, the wing is pivoted in slide bearings. A controllable motor allows the rotation of the wing in an almost sinusoidal motion around its quarter chord. The testbed can be mounted in the windtunnel under arbitrary yaw angles with two large endplates on either side of the wing adjusted parallel to the freestream. A sketch of the testbed is shown in Fig. 1.

The testsection for the performed experi-

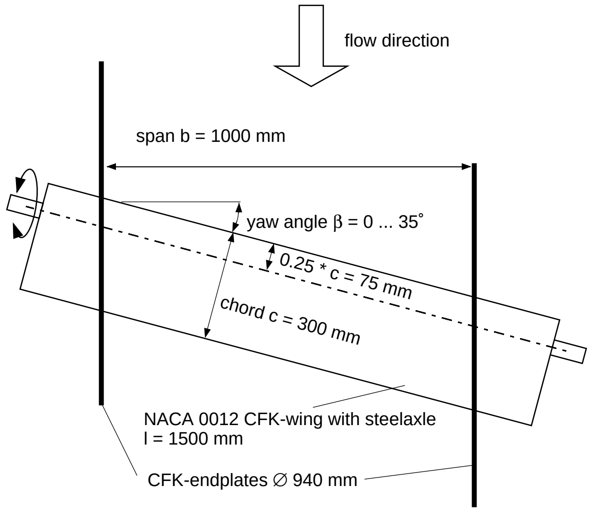

Fig. 1 Swept wing for dynamic stall tests

ments was situated midway between the two endplates. Control measurements had found that the nonuniformness along the span due to disturbances from the endplates is small. Tab. 1 shows an overview of the parameters for the performed experiments. The presented results were obtained by phase-locked averaging over approximately 200 cycles. For the turbulent measurements a trip wire has been placed at the leading edge to ensure full turbulent conditions during the cycle.

The flow fields were measured with an advanced eight-hot-wire probe based on an earlier probe development for turbulent two-dimensional separated flows [12]. This newly developed probe enables unique velocity measurements in turbulent three-dimensional flow without any restrictions pertaining to the main flow direction [7, 6]. The probe consists of four normal hot-wires and two direction- and heating-wire pairs which detect the flow direction and eliminate the equivocation occurring with usual hot-wire probes.

4 Numerical Method

For the comparative numerical simulation, the unsteady Reynolds averaged Navier-Stokes solver FLOWer [10] was used which permitted the calculation of an infinite swept wing on a two dimensional grid. The simulation was carried out

k	0.15	0.22	0.3	0.45	0.22 turb.	0.3 turb.
$f[Hz]$	1.0	1.5	2.0	3.0	1.5	2.0
Re	$0.25 \cdot 10^6$					
$\alpha(t)[^\circ]$	$10^\circ \pm 10^\circ$					

Table 1 Parameters of the performed test series

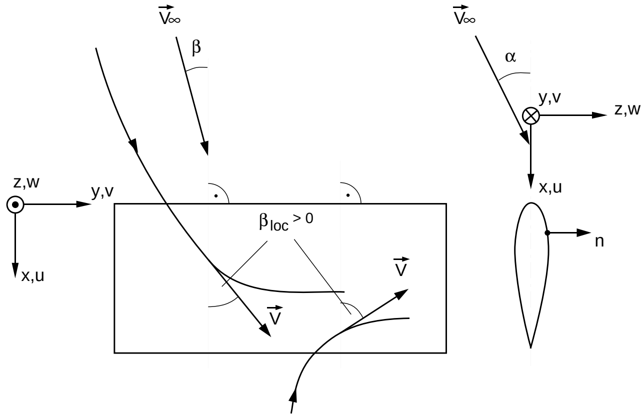

Fig. 2 Definition of the displacement angle β_{loc}

on a 416x104 cell C-grid. A study surveying the grid dependencies for steady cases showed no significant change in the solutions when using a finer grid. A complete oscillation was calculated in 100 time steps using the implemented dual time stepping scheme [9]. A finer resolution of 200 time steps per cycle for a chosen test case revealed no relevant differences to the coarser temporal resolution. All calculations were carried out as full turbulent simulations using the k-ω model proposed by Wilcox [17]which showed better agreement with experimental data [16, 5] than the Baldwin-Lomax algebraic model [1]. The free stream Mach number was set to $Ma = 0.1$. Verification showed that the maximum attained Mach number was below $Ma = 0.3$ at all times for all considered cases.

5 Three Dimensional Dynamic Stall

As an example the evolution of the dynamic stall is presented here for the reduced frequency $k = 0.22$. The other considered cases show the same features, yet with a different temporal evolution. The phase t/T denotes the relative nondimensional time since passing the lower dead center at an incidence angle of $\alpha = 0^\circ$. The upper dead center at $\alpha = 20^\circ$ is reached at $t/T = 0.5$. The velocity component in the spanwise direction is visualized by the displacement angle β_{loc}, defined as depicted in Fig. 2. A positive value for β_{loc} means v-components in the positive y-direction and vice versa.

5.1 Experimental Results

Starting at the lower dead center at $t/T = 0$ no signs of separation are visible in the experiment during the wing's upstroke motion. With increasing incident angles a zone with high velocities develops above the nose region. In the trailing edge region decreasing velocities with a tendency towards higher displacement angles related to a growing boundary layer are visible. Nevertheless no reverse flow occurs up to $t/T = 0.47$ at $\alpha = 19.8^\circ$, which is well above the incidence angle of static stall.

First signs of the dynamic stall process evident in the experimental data appear at $t/T = 0.47$, as can be seen in Fig. 3a. The onset of the dynamic stall vortex is visible in the vicinity of the wall above quarter chord. The start is marked by a vanishing chordwise velocity. In conjunction with the vanishing velocity a cross flow with displacement angles near 90° appears, Fig. 4a. At the trailing edge region near the wall the chordwise velocity has increased whereas in the wall remote region the velocity has further diminished. A reversed effect can be noticed in the nose region. For the upstream positions velocities in the vicinity of the surface are decreasing with time until the wing reaches the upper dead center. Simultaneously velocities off the wall increase.

After the first appearance of the reverse flow near the quarterchord, the vortex increases in size and spreads further up- and downstream along the upper surface. Shortly before reaching the upper dead center at $t/T = 0.49$ it covers almost two thirds of the surface. However separation has not occurred yet as the flow is still attached at the trailing edge, as can be seen in the resulting dis-

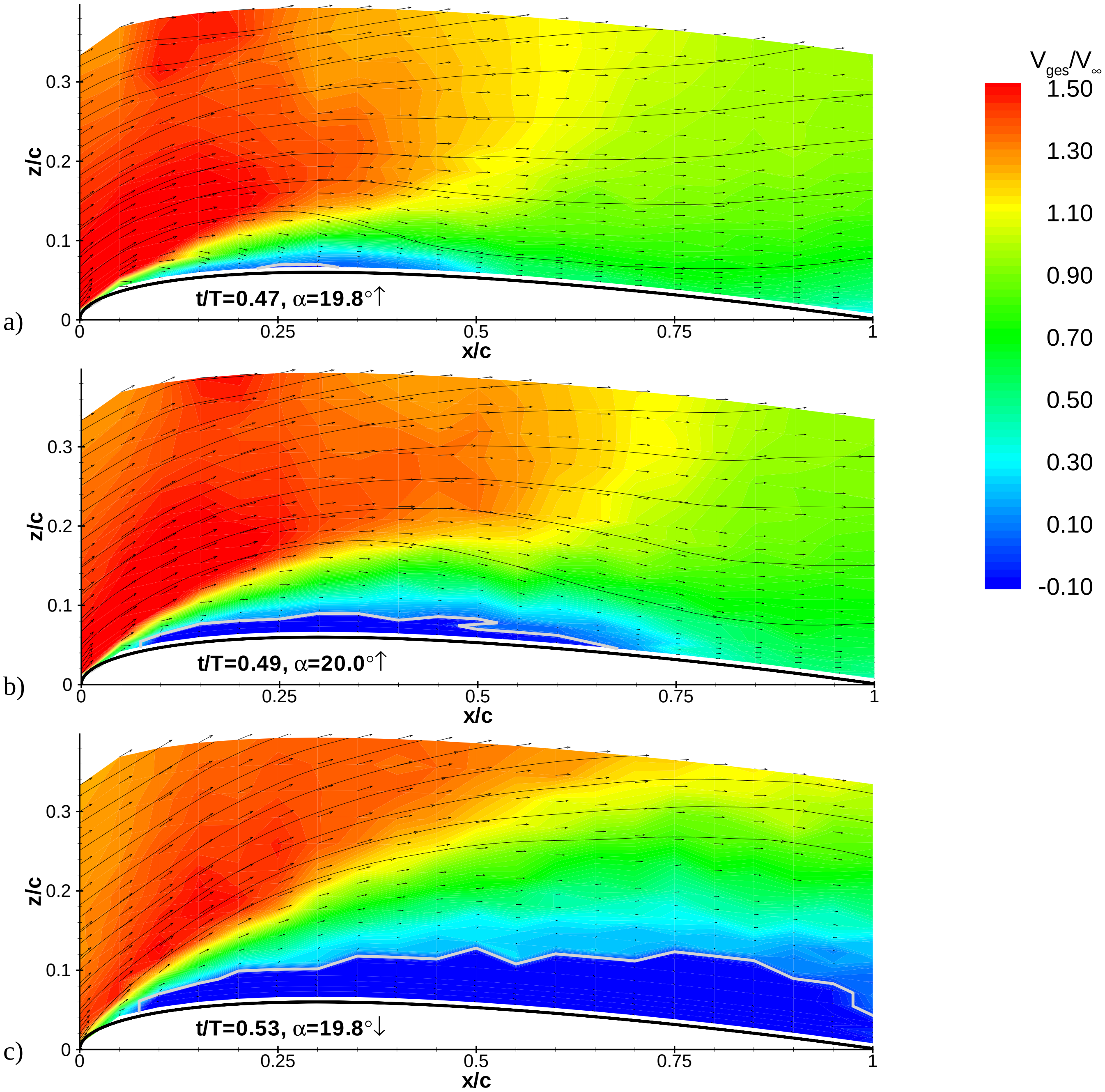

Fig. 3 Distribution of the total velocity from experiment, gray line separates reverse flow

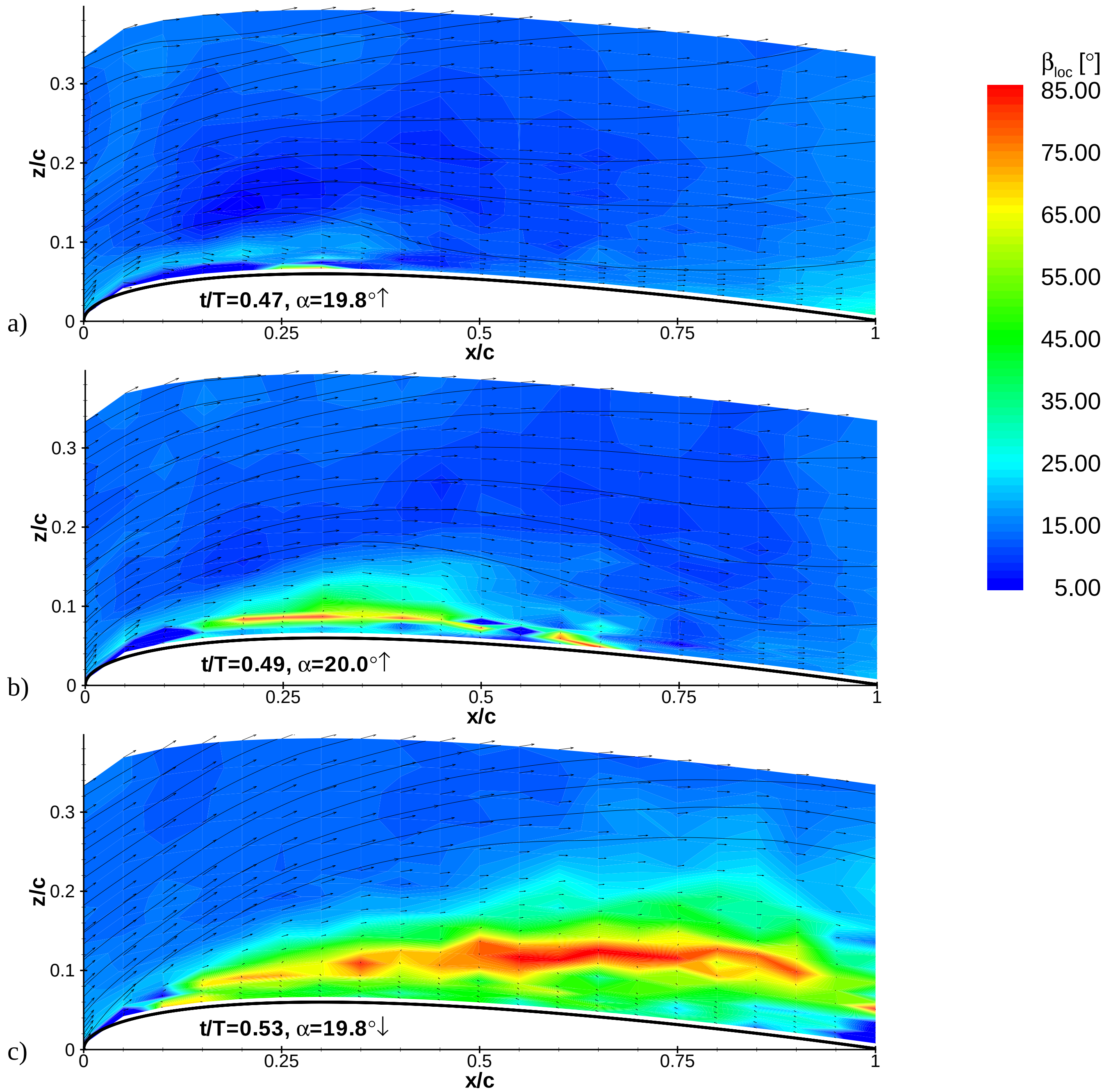

Fig. 4 Distribution of the local displacement angle from experiment

placement angles, Fig. 4b and the total velocity in Fig. 3b. A surface with cross flow has developed, which separates from the surface and encloses the reverse flow.

At $t/T = 0.53$ in Fig. 3c the reverse flow has spread all over along the upper surface. The extent of this region with reverse flow normal to the wall has drastically increased. Especially the magnitude of the velocity in the trailing edge region has decreased and the full separated state has occurred. Large displacement angles are visible at the trailing edge marking a shear layer, Fig. 4c.

The separated region grows until $t/T = 0.55$, where it reaches its largest extent. In subsequent phases the flow field slowly reverts to attached flow beginning at the the nose, with the attachment point moving towards the trailing edge.

5.2 Computational Results

Numerical and experimental data show congruent features, although the computational results exhibit a significant phase shift towards earlier times t/T, see Fig. 8.

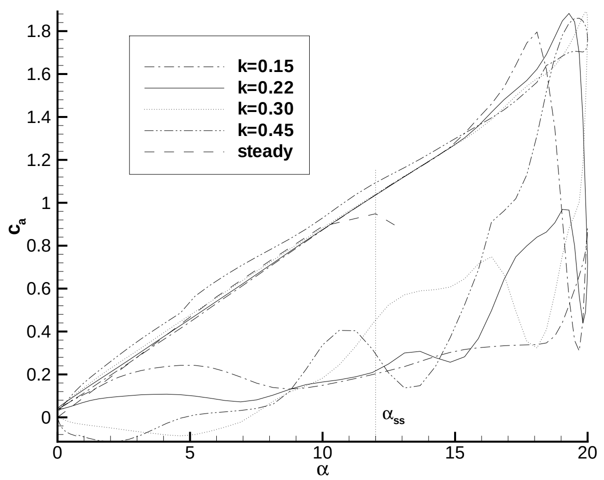

Fig. 5 c_a-α

Moreover a reverse flow very close to the surface can be noticed before the inception of the dynamic stall vortex. This effect cannot be observed in the experiment, due to the limitations arising from the probe size and the surface clearance required. Closer inspection of all considered computational cases revealed that this reverse flow appeared independently from the reduced frequency at $t/T = 0.26$ and the chord position $x/c = 0.045$. Up to this moment no reverse flow occurred down- or upstream from this point.

During the upstroke motion the lift cycles show almost no deviation from the steady case, Fig5. Even above α_{ss} the cycles follow the linear quasi steady progression with occurrence of the reverse flow having neither a significant impact on the lift nor on the pressure distribution. First divergences from this common trend do occur not until the start of the dynamic stall vortex, visible in the cycles as a significant rise in the lift slope. This quasi steady behavior was also observed in many two dimensional experiments [2, 4] as well as in experiments on swept wings [13].

5.3 Evolution of the Dynamic Stall

Both of the above described results - the numerical and the experimental - cases can be used to explain the onset of the dynamic stall and the affiliated vortex. The description given is also valid for the two-dimensional flow, as it is only a special case of the infinite swept wing, [6]. Italics in the following paragraphs denote features of the three-dimensional case only. The formation of the dynamic stall is separated into four stages as depicted in Fig. 6.

- With increasing angle of attack a strong suction peak evolves at the leading edge, Fig. 6a. *Due to the spanwise pressure gradient caused by the yaw angle the velocity vectors are rotated into the spanwise direction in regions of decelerated flow in chordwise direction and vice versa. For the positions near the leading edge in Fig. 4a in the near wall region a lower displacement angle than the global yaw angle of* $15°$ *can be observed.*

- After passing the angle of static stall α_{ss} a reverse flow starts in the nose region due to a steep pressure rise appearing after the suction peak, Fig. 6b. This flow reversal can move upstream without separa-

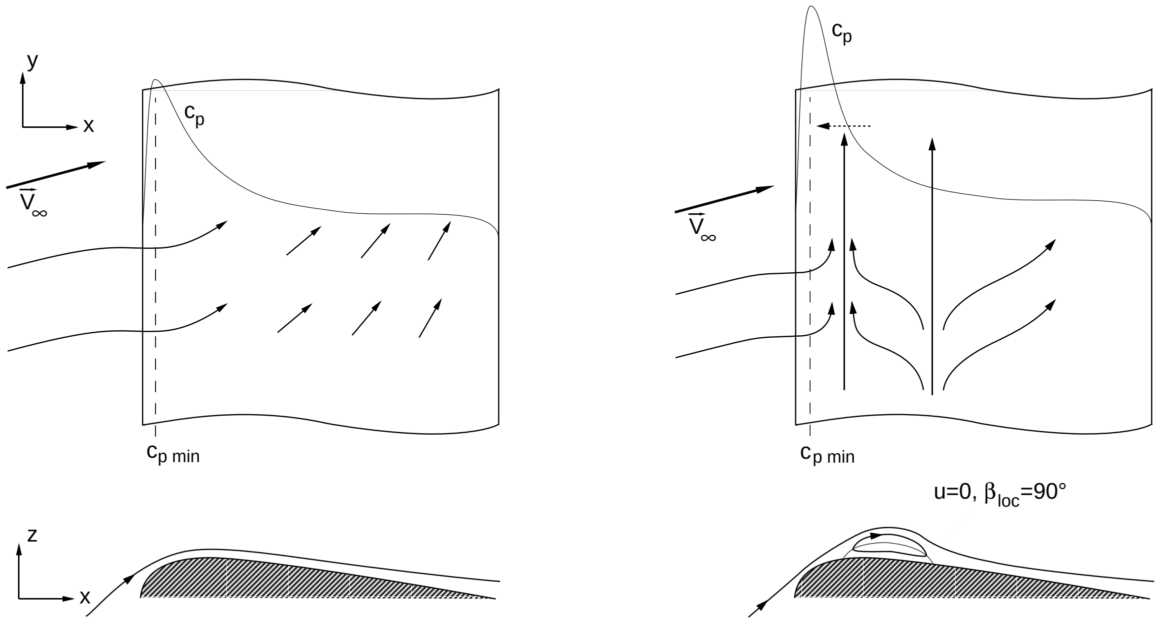

a) Attached flow

b) Reverse flow on the surface

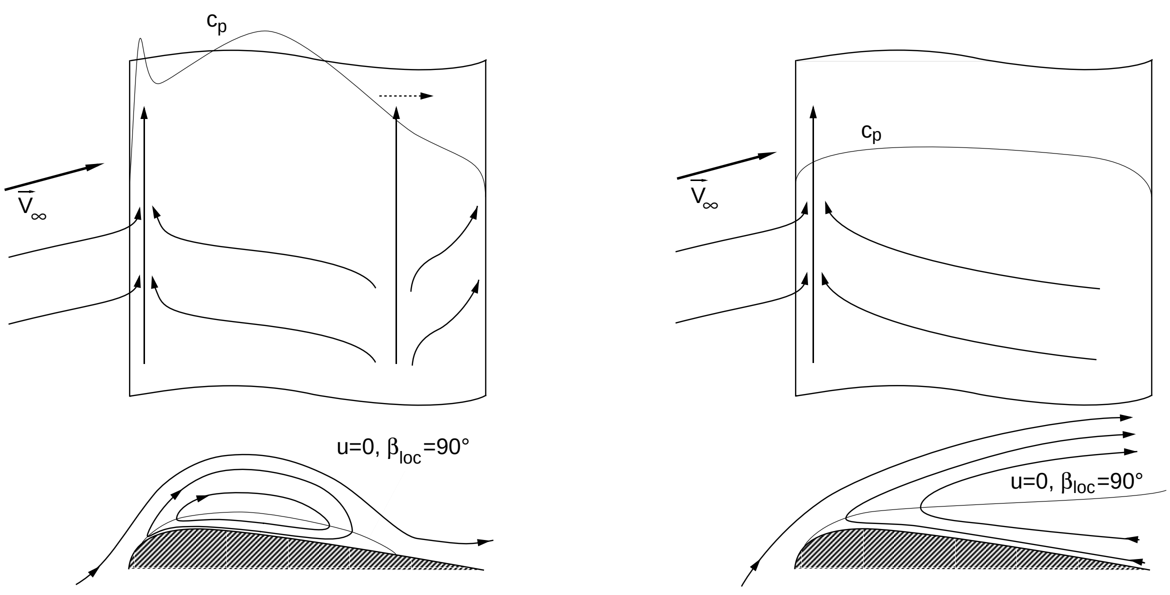

c) Inception of the dynamic stall vortex

d) Vortex bursting

Fig. 6 Stages of the dynamic stall, wall streamlines and cuts tion as long as the reverse velocity magnitude is lower than the upstream movement of this region [15, 16] and cannot be observed in surface pressure measurements as it does not have a significant impact on the pressure distribution. *In three-dimensional flow, a layer of cross flow i.e. displacement angles of almost* 90° *appears, enclosing the region of reverse flow.*

It can easily be seen from the equations of momentum and mass conservation for the incompressible unsteady boundary layer

$$\begin{aligned}
\frac{\partial u}{\partial t}+u\frac{\partial u}{\partial x}+v\frac{\partial u}{\partial y}+w\frac{\partial u}{\partial z} &= -\frac{\partial p_a}{\partial x}+\mu\frac{\partial^2 u}{\partial z^2}\\
\frac{\partial v}{\partial t}+u\frac{\partial v}{\partial x}+v\frac{\partial v}{\partial y}+w\frac{\partial v}{\partial z} &= -\frac{\partial p_a}{\partial y}+\mu\frac{\partial^2 v}{\partial z^2}\\
\frac{\partial u}{\partial x}+\frac{\partial v}{\partial y}+\frac{\partial w}{\partial z} &= 0 \qquad (1)
\end{aligned}$$

that no unsteady contribution from the pressure outside the boundary layer appears. Consequently, no contributions from the pressure's rate of change or the absolute pressure level to the development of the boundary layer take place. Moreover for the infinte swept wing all derivatives of the spanwise direction must vanish and the equations are reduced to a quasi two-dimensional form:

$$\begin{aligned}
\frac{\partial u}{\partial t}+u\frac{\partial u}{\partial x}+w\frac{\partial u}{\partial z} &= -\frac{\partial p_a}{\partial x}+\mu\frac{\partial^2 u}{\partial z^2}\\
\frac{\partial v}{\partial t}+u\frac{\partial v}{\partial x}+w\frac{\partial v}{\partial z} &= -\frac{\partial p_a}{\partial y}+\mu\frac{\partial^2 v}{\partial z^2}\\
\frac{\partial u}{\partial x}+\frac{\partial w}{\partial z} &= 0. \qquad (2)
\end{aligned}$$

This has two consequences: On one hand the topology of the boundary layer separation for the swept case must fulfill the criteria given by Ranke [15, 16] when mapped onto the x-z plane. The evolving crossflow has no direct impact on the separation topology. On the other hand the development and the movement of the described region is almost independent from the reduced frequency because of the the quasi

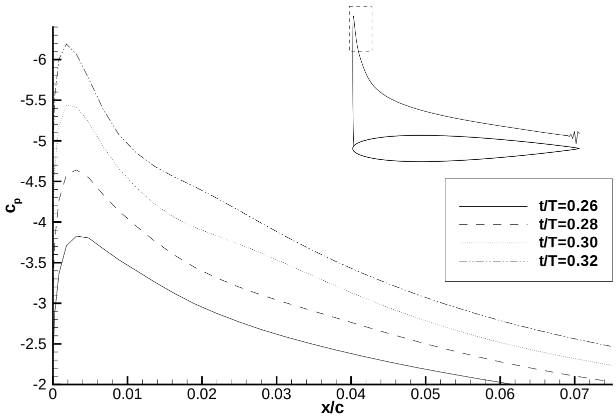

Fig. 7 Distribution of pressure in the the nose region after the start of reverse flow, $\beta = 15^\circ$, $k = 0.22$

steady behavior of the pressure distribution preceding the vortex inception. The chordwise pressure gradients in the nose region are almost constant which can be seen in Fig. 7 with the parallel progression of pressure coefficient.

- The upstream movement of the reverse flow continues until it reaches the point of minimum pressure where it stops, Fig. 6c. Consequently the reverse flow components will become greater than the movement of the region itself and the boundary layer separates. This boundary layer separation at the nose is the onset of the dynamic stall vortex. *Due to the crossflow developing in the reverse flow region, the movement in the three-dimensional case is slower than for the two-dimensional one. Therefore the point of separation is reached at a later phase time* t/T. *This results in a comparable cycle to a non swept case with a higher reduced frequency. As stated before, this effect was first observed by Hilaire and Carta [8] but could not be explained up till now.*

- Due to this impulsive large growth of boundary layer thickness related to its separation, the vortex now develops. It draws energy from the outer flow with high velocities and transports it into the trailing edge region and the near wall layer. The lift is further increased by keeping the flow attached at the trailing edge. Gradually the vortex increases in size and spreads downstream along the chord. Finally the vortex bursts, Fig 6d, and a sharp drop in the lift cycle occurs. The flow now has entered the fully separated stage. In subsequent phases the field slowly reverts to attached flow, starting at the leading edge with the reattachment point moving downstream.

5.4 Consequences

The above postulated independence of the reverse flow movement is clearly visible in Fig. 8. For higher reduced frequencies the onset of the vortex must occur at later times with a linear dependence of k and for slower movements earlier. The computational results show the above described phase shift towards earlier times, nevertheless exhibiting the same linear behavior with the same slope. The turbulent measurements are in better agreement with the computational results than the ones with natural transition, yet still showing a strong discrepancy. As stated above in the computational results the reverse flow starts at $t/T = 0.26$, which connotes an incidence angle of $10.6°$. This early onset of flow reversal seems very unlikely and is attributed to the turbulence model's deficiency to predict unsteady flows correctly.

For incidence angle movements which have the same progression of $\dot{\alpha}(t)$ between the angle of static stall α_{ss} and the inception of the dynamic stall vortex, the resulting lift cycles should match in that region. This conforms with observations made by Ericsson [4]. As demonstrated, the separation process starts when passing the angle of static stall. The development of the flow reversal is at first independent of the reduced frequency and the "history" of the movement, because the prevailing outer flow and the pressure gradients follow a quasi steady trend. Consequently the vortex inception and bursting must occur at the same incidence angle and exhibit the same characteristics.

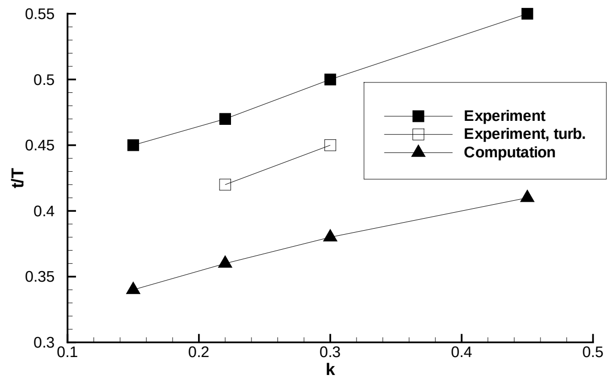

Fig. 8 Vortex inception with varying reduced frequency

6 Conclusions

As demonstrated in the preceding paragraphs, the onset and evolution of dynamic stall can be attributed to boundary layer effects only. The outer flow and the surface pressure distribution inhibit a quasi-steady progression until the vortex starts.

Numerical results are principally in good agreement with the experiment but show a significant phase shift to lower incident angles because. This difference can be attributed to the used turbulence model which is apparently unable to predict the onset of reverse flow exactly. This flow reversal appears here at very unlikely early phases t/T even before reaching α_{ss}. Anyhow the aforementioned phase shift of the numerical results remains constant for all considered cases.

The proposed explanation for the onset of dynamic stall and the vortex inception in incompressible flow does not rely on any assumptions about laminar or turbulent conditions. Effects of compressiblity should not have a severe impact onto the mechanism leading to inception of the vortex, as long as they are not dominating the flow.

The process of dynamic stall can be divided into four stages. Flow reversal in the leading edge region appears during upstroke motion when the wing passes through the incident angle of static stall. This flow reversal can move upstream without causing separation and significant disturbances of the surface pressure distribution. When this region of flow reversal reaches the location of minimum pressure at the leading edge, the propagation of the flow reversal ends. Boundary layer separation takes place and the dynamic stall vortex forms. The propagation velocity of the flow reversal can be seen independent from the reduced frequency of the movement due to the quasi-steady behavior of the outer flow. This causes a linear dependency of the nondimensional time t/T of vortex inception from the reduced frequency. This phenomenon can be supported by experimental and numerical results at various reduced frequencies. Due to the crossflow occurring on swept wings, the movement of the flow reversal in the chordwise direction is slower than in the two-dimensional case and leads to a delayed inception of the dynamic stall vortex. This results in a lift cycle comparable to an unswept case at a higher reduced frequency.

References

[1] Baldwin B. S and Lomax H. Thin Layer Approximation and Algebraic Model for Separated Turbulent Flows. *Proc AIAA 16th Aerospace Meeting*. Huntsville, 1978.

[2] Carr L, McAlister K, and McCroskey W. Analysis of the Development of Dynamic Stall Based on Oscillating Airfoil Experiments. Technical Report NASA-TN-8382, NASA, Jan. 1977.

[3] Carta F. O. Analysis of Oscillating Pressure Data including Dynamic Stall Effects. Technical Report NASA-CR-2394, NASA, May 1974.

[4] Ericsson L. E and Reding J. P. Fluid Mechanics of Dynamic Stall. Part I. Unsteady Flow Concepts. *Journal of Fluids and Structures*, Vol. 2, pp 1–33, 1988.

[5] Galbraith R, Gracey M. W, and Gilmour R. Collected data for tests on a naca 0012 aerofoil. Technical Report Report 9208, University of Glasgow, Department of Aerospace Engineering, Feb. 1992.

[6] Henkner J. *Phänomene der instationären Grenzschichtablösung bei schiebenden Tragflächen*. PhD thesis, Lehrstuhl f. Fluidmechanik, Technische Universität München, 1999.

[7] Henkner J and Ranke H. Unsteady Boundary Layer Separartion on Swept and Unswept Wings in Sinusoidal Dynamic Stall Motion. *Proc New Results in Numerical and Experimental Fluid Mechanics*, pp 181–188. Vieweg Verlag, 1996.

[8] Hilaire A and Carta F. Analysis of Unswept and Swept Wing Chordwise Pressure Data from an Oscillating NACA 0012 Airfoil Experiment, Volumen I. Technical Report NASA-CR-3567, NASA, 1983.

[9] Jameson A. Time Dependent Calculation Using Multigrid, with Applications to Unsteady Flows past Airfoils and Wings. Technical Report AIAA-91-1596, AIAA, 1991.

[10] Kroll N. *FLOWer, Installation And User Handbook*, 1998.

[11] Laschka B. On some Fundamentals of Unsteady Viscous Flows. *Proc La Sapienza*. Universita degli Studi di Roma Dipartimento Aerospaziale, 1994.

[12] Laschka B, Ranke H, and Breitsamter C. Application of Unsteady Measurement Techniques to Vortical and Separated Flows. *ZfW Journal*, 1994.

[13] Patterson A, Rymarz P, and B.R.Ramaprian. Surface Pressure Measurements on a Pitching Swept Wing in a Water Channel. *AIAA Journal*, Vol. 33, No 10, pp 1871–1879, Oct. 1995.

[14] Raffel M, Kompenhans J, and Wernert P. Investigation of the Unsteady Flow Velocity Field above an Airfoil Pitching under Deep Dynamic Stall Conditions. *Experiments in Fluids*, Vol. 19, pp 103–111, 1995.

[15] Ranke H. *Instationäre Grenzschichtablösung in ebener, kompressibler Strömung*. PhD thesis, Lehrstuhl f. Fluidmechanik, Technische Universität München, 1994.

[16] Ranke H. Unsteady separation in two-dimensional turbulent flows. *Proc ICAS 94, 19th Congress of the International Council of the Aeronautical Sciences, Anaheim, California, Paper 94–4.5.1*, Sep. 1994.

[17] Wilcox D. C. Comparison of Two-equation Turbulence Models for Boundary Layers with Pressure Gradient. *AIAA Journal*, Vol. 31, No 8, pp 1414–1421, 1993.